Diagn Interv Radiol 2025; DOI: 10.4274/dir.2025.243148

NEURORADIOLOGY

PICTORIAL ESSAY

Clival and paraclival pathologies: imaging features and differential diagnosis

Ahmet Bozer[1]
Yeliz Pekçevik[1,2]

[1]İzmir City Hospital, Clinic of Radiology, İzmir, Türkiye

[2]University of Health Sciences Türkiye, İzmir University Faculty of Medicine, Department of Radiology, İzmir, Türkiye

ABSTRACT

Clival and paraclival pathologies encompass a broad spectrum of benign and malignant lesions, necessitating accurate imaging for precise diagnosis and management. Magnetic resonance imaging and computed tomography are pivotal in evaluating these lesions, facilitating differentiation, and guiding therapeutic decisions. This study reviews the imaging characteristics, differential diagnoses, and clinical significance of clival and paraclival pathologies.

KEYWORDS

Clivus, computed tomography, chordoma, magnetic resonance imaging, skull base

The clivus, a sloping skull base bone, supports the brainstem and separates the posterior cranial fossa from the sphenoid sinus. It comprises the basisphenoid and basiocciput, which fuse in adulthood. In children, the spheno-occipital synchondrosis, a joint aiding skull base growth, separates these structures and fuses by the late teens to mid-twenties.[1] The central location of the clivus and its proximity to critical neurovascular structures make it vital in both normal and pathological conditions, especially in trauma or skull base lesions.

Clival and paraclival pathologies encompass a wide range of benign and malignant lesions (Table 1). Due to the proximity of the clivus to the brainstem, cranial nerves, and major vessels, a precise imaging diagnosis is essential. Magnetic resonance imaging (MRI) and computed tomography (CT) are essential for localizing, assessing, and differentiating pathologies such as neoplasms, inflammation, and congenital abnormalities, guiding targeted treatment. This essay highlights the imaging features and diagnostic approaches for clival and paraclival lesions. Informed consent was obtained from the patients for the use of the clinical and imaging data included in this review.

Table 1. Classification of clival and paraclival pathologies

Category	Subtype	Pathologies
Primary clival lesions	**Benign lesions**	Benign bone lesions, benign-appearing notochordal lesions
	Malignant lesions	Chordoma, chondrosarcoma, plasmacytoma/multiple myeloma, metastasis
Paraclival pathologies	**Infectious and inflammatory lesions**	Skull base osteomyelitis, IgG4-related disease
Secondary clival lesions: pathologies extending to the clivus	**Head and neck pathologies**	Nasopharyngeal carcinoma, sinonasal malignancies
	Intracranial pathologies	Meningioma, pituitary neuroendocrine tumor

Corresponding author: Ahmet Bozer

E-mail: drahmetbozer@gmail.com

Received 02 December 2024; revision requested 01 January 2025; last revision received 29 January 2025; accepted 09 February 2025.

Epub: 27.03.2025

Publication date:

DOI: 10.4274/dir.2025.243148

You may cite this article as: Bozer A, Pekçevik Y. Clival and paraclival pathologies: imaging features and differential diagnosis. *Diagn Interv Radiol.* 27 March 2025. DOI: 10.4274/dir.2025.243148 [Epub Ahead of Print].

Imaging techniques

CT and MRI serve as complementary techniques in evaluating clival and paraclival pathologies. CT is superior for the detailed analysis of bony structures, the identification of calcifications, and the evaluation of their patterns. Thin-slice axial and coronal reconstructions are particularly valuable for assessing bone erosion and destruction.

MRI offers superior soft tissue contrast and is essential for evaluating intracranial extensions and bone marrow signal abnormalities. It also plays a critical role in assessing the treatment response and follow-up. Standard multiplanar T1-weighted (T1W) and T2-weighted (T2W) sequences are used alongside post-contrast T1W sequences to evaluate lesion enhancement. Diffusion-weighted imaging and apparent diffusion coefficient (ADC) mapping assist in the differential diagnosis.

Advanced sequences such as fast imaging employing steady-state acquisition (FIESTA) and constructive interference in steady state (CISS) provide high spatial resolution with submillimeter section thickness. These sequences enhance the visualization of small lesions and structures, especially those with high T2 signal intensity, such as cerebrospinal fluid (CSF). Their multiplanar reconstruction capabilities are valuable for the detailed imaging of the brainstem, small cystic lesions, and the surrounding neural structures. These sequences may also be used with contrast, which is useful for the differential diagnosis and the further evaluation of the details and extension of the lesions. The integration of CT and MRI with these advanced imaging techniques enables a comprehensive evaluation of clival and paraclival pathologies. Additionally, fluorodeoxyglucose positron emission tomography (FDG PET)/CT can complement CT and MRI, particularly for staging purposes and the assessment of the treatment response.

Main points

- Clival and paraclival pathologies, which extend into the clivus, are categorized into primary clival lesions (benign and malignant), paraclival infectious/inflammatory conditions, and secondary clival lesions.
- High-resolution sequences, such as constructive interference in steady state/fast imaging employing steady-state acquisition, diffusion-weighted imaging, and post-contrast sequences, are valuable for the differential diagnosis of clival lesions.
- Although chordomas and chondrosarcomas have overlapping imaging features, higher apparent diffusion coefficient values in chondrosarcomas may aid in their differentiation.
- The radiological and pathological features of benign notochordal cell tumors overlap with those of clival chordomas, justifying the use of the term "benign-appearing notochordal lesions," which should be monitored with imaging every 6 months.

Normal anatomy of the clivus

The clivus is bordered superiorly by the dorsum sellae and sella, inferiorly by the foramen magnum, and laterally by the petroclival fissure, which includes the petro-occipital synchondrosis, petrous temporal bone, and internal carotid artery. Anteriorly, it adjoins the sphenoid sinus and nasopharynx, and posteriorly, the prepontine and premedullary cisterns, containing the brainstem (Figure 1).

The clivus is best visualized on a sagittal T1W MRI. It shows age-related changes in the bone marrow signal caused by the increasingly yellow (fatty) marrow, leading to T1W hyperintensity. A normal clival signal is typically isointense or hyperintense relative to the pons, and T1W hypointensity warrants suspicion. Clival marrow heterogeneity may manifest as hypointense foci. The T1W signal is categorized as follows: grade 1 indicates a low signal, occupying >50%; grade 2 covers 20%–50%; and grade 3 exhibits a high signal, with a low signal occupying <20% (Figure 2). Mild enhancement is often noted in grade 1 T1W signals.[2]

Primary clival lesions

Benign lesions

Fibrous dysplasia

Fibrous dysplasia is a benign fibro-osseous condition, in which normal bone is replaced with fibrous tissue. It affects all ages but is commonly diagnosed in childhood or early adulthood, with no gender predilection. Although usually sporadic, it can be linked to syndromes such as McCune–Albright and Mazabraud or isolated endocrinopathies.[3]

Most cases (70%–80%) are monostotic, commonly involving craniofacial bones, long bones, and the spine.[4] Clival involvement is rare, with only 44 cases reported in a 2023 review.[5] Diagnosis is primarily radiological, with histopathology reserved for symptomatic or atypical monostotic cases.

On imaging, CT typically reveals an expansile, ground-glass intramedullary lesion diagnostic of fibrous dysplasia. On MRI, it appears hypointense on T1W signals and exhibits a variable T2W signal with moderate-to-marked post-contrast enhancement (Figure 3).

Management typically involves observation and bone quality maintenance. Imaging should evaluate benign matrix transformation (e.g., aneurysmal bone cyst-like changes, myxoid degeneration) and malignant features, such as fractures, cortical destruction, aggressive periosteal reactions, marrow edema, solid masses, or soft tissue components.

Differential diagnoses include other fibro-osseous lesions, Paget's disease, and primary clivus lesions such as intraosseous

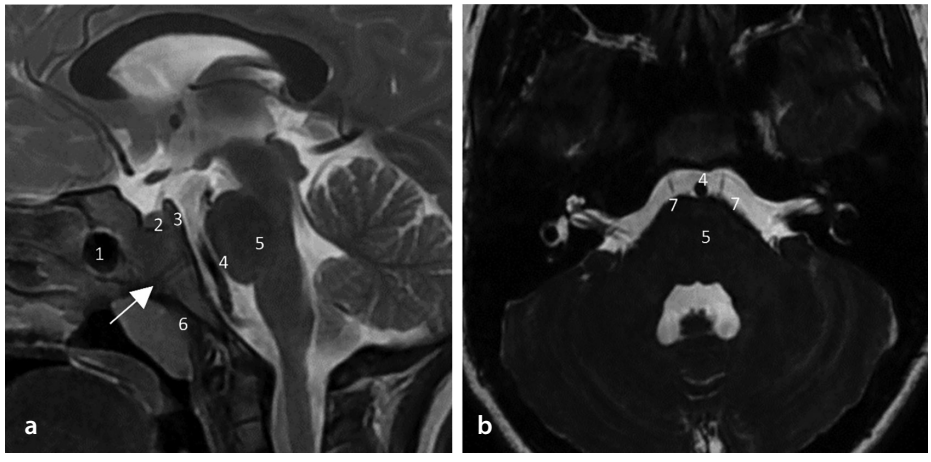

Figure 1. Magnetic resonance imaging anatomy of the clivus in a 4-year-old male pediatric patient. Sagittal T2-weighted (T2W) image **(a)** and axial heavily T2W image **(b)**, demonstrating the key anatomical structures. The spheno-occipital synchondrosis (arrow), located between the basisphenoid and basiocciput, is clearly visible. The key adjacent structures are labeled: 1. Sphenoid sinus, 2. pituitary gland, 3. dorsum sella, 4. basilar artery, 5. pons, 6. nasopharynx, 7. abducens nerve.

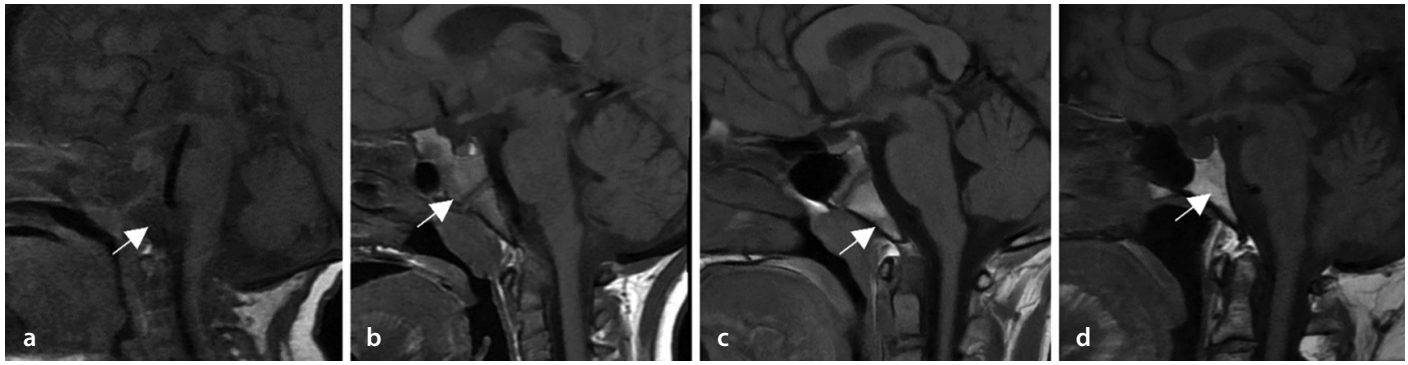

Figure 2. Signal changes in clival bone marrow on non-fat-suppressed T1-weighted (T1W) magnetic resonance imaging. Sagittal T1W images **(a-d)** without fat suppression from patients at 6 months **(a)**, 4 years **(b)**, 14 years **(c)**, and adulthood **(d)** are shown. The images demonstrate the gradual replacement of red bone marrow (hypointense) by fatty bone marrow. The signal intensity changes are graded as grade 1 **(a)**, grade 2 **(b)**, and grade 3 **(c, d)**, as indicated by the arrows.

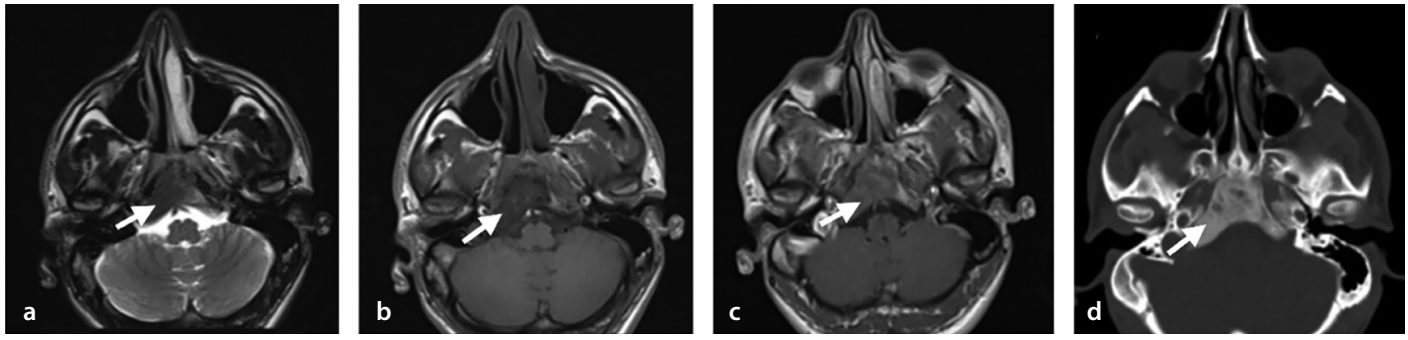

Figure 3. Imaging features of a lesion consistent with monostotic fibrous dysplasia in the clivus in a 31-year-old male patient. An incidental lesion in the clivus, appearing hypointense on T2-weighted **(a)** and T1-weighted (T1W) **(b)** sequences. The lesion is intramedullary in location and mildly expansile (arrow). On post-contrast T1W imaging **(c)**, the lesion exhibits moderate enhancement, raising suspicion for fibrous dysplasia, and a computed tomography (CT) scan was recommended. The CT scan **(d)** confirms a well-defined, mildly expansile lesion with ground-glass density, supporting the diagnosis of fibrous dysplasia (arrow).

meningioma and chordoma. Paget's disease may appear radiologically similar to fibrous dysplasia, but it primarily occurs in older individuals, whereas fibrous dysplasia can be seen across a broader range of age groups. Intraosseous meningiomas tend to be less extensive than fibrous dysplasia, with less bony remodeling. Chordoma can be easily distinguished from fibrous dysplasia because of its lytic destructive appearance, possible expansile solid component, and more pronounced contrast enhancement.

Benign-appearing notochordal lesions

Ecchordosis physaliphora and benign notochordal cell tumors

Ecchordosis physaliphora is a benign hamartomatous lesion from ectopic notochordal remnants. It is non-proliferative, non-invasive, and asymptomatic but can present with symptoms such as headache, CSF leaks, or diplopia. Ecchordosis physaliphora is classified as a benign notochordal cell tumor in current pathology systems.[6]

The radiological and pathological features of BNCT overlap with those of clival chordoma, making the term "benign-appearing notochordal lesions" preferable for EP/BNCT.[7] MRI reveals T1-hypointense and T2-hyperintense lesions, similar to chordomas, although chordomas are often enhanced with contrast. The FIESTA and CISS sequences are valuable for identifying small intracranial lesions, providing high-resolution images for multiplanar reconstruction. These sequences are recommended for diagnosing and classifying clival lesions.[8]

Benign notochordal cell tumors remain stable during follow-up, whereas low-grade chordomas exhibit slow growth, although differentiation remains challenging. These lesions can be defined as "benign-appearing notochordal lesions" and should be monitored through imaging at 6-month intervals.[7]

Surgical considerations include tumor size (<3 cm), growth, local invasion, bony erosion, patient age (<30 years), symptoms, and patient preference (Figure 4).

Malignant lesions

Chordomas

Chordomas, arising from notochord remnants, account for 1%–4% of bone malignancies and 0.5% of primary intracranial central nervous system tumors.[9] Cranial chordomas represent approximately 40% of cases, with sacral and spinal forms being less common. They predominantly affect adults, especially men, with peak incidence in the 70–80-years age range.[10]

Radiologically, CT shows a lytic, expansile mass with secondary calcifications caused by sequestration. On MRI, chordomas appear hyperintense on T2W images and hypointense on T1W images, occasionally with hemorrhagic foci. Post-contrast imaging often reveals a honeycomb pattern (Figures 5 and 6).

Despite their slow growth and low-grade histology, chordomas are locally invasive, recur frequently, and are classified as malignant. Treatment typically involves surgery with adjuvant radiotherapy. Surgical resection is critical for progression-free and overall survival.

Differential diagnoses include chondrosarcoma, metastasis, plasmacytoma, and, rarely, jugular paraganglioma. No conventional CT or MRI feature reliably distinguishes chordomas from chondrosarcomas; how-

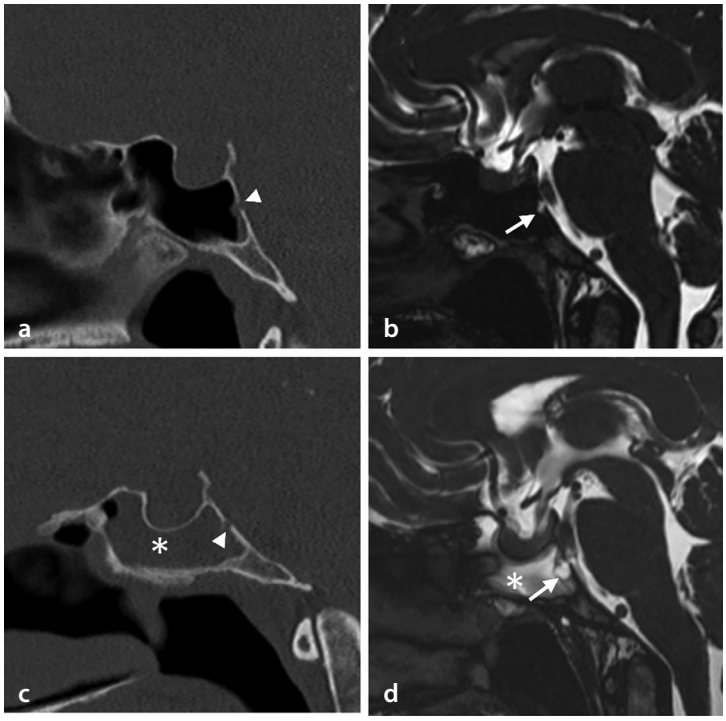

Figure 4. Benign-appearing notochordal lesion causing cerebrospinal fluid rhinorrhea and follow-up imaging in a 45-year-old female patient. Initial evaluation with computed tomography (CT) **(a)** reveals a clival defect (arrowhead) and a hyperintense focal clival lesion (arrow) on constructive interference in steady-state (CISS) imaging **(b)**. The patient declined surgical intervention and, after 4 years, presented with exacerbated symptoms. Follow-up CT **(c)** and CISS imaging **(d)** demonstrate fluid accumulation in the sphenoid sinus (asterisk) and an increase in the size of the clival lesion (arrow).

ever, ADC values, enhancement patterns, and bone changes may help differentiate the two, as they often share overlapping imaging features. Chondrosarcomas typically exhibit higher ADC values than chordomas.[11] The high T2 signal intensity of chondroid lesions helps differentiate them from metastases and plasmacytomas, whereas poorly differentiated chordomas may exhibit a low T2 signal. Paragangliomas have a distinct salt-and-pepper appearance, flow voids, and moth-eaten bone destruction.

Chondrosarcomas

Skull base chondrosarcomas are rare tumors that typically arise from the petro-occipital synchondrosis, which is believed to explain their usual off-midline location. However, 10%–30% may occur at the midline.[12] These slow-growing tumors often present with brainstem or cranial nerve compression symptoms.

On CT, these tumors may exhibit typical chondroid calcifications (popcorn-like or ring-and-arc patterns) and appear as destructive, heterogeneous masses. On MRI, they are hypointense on T1W images, hyperintense on T2W images, and demonstrate

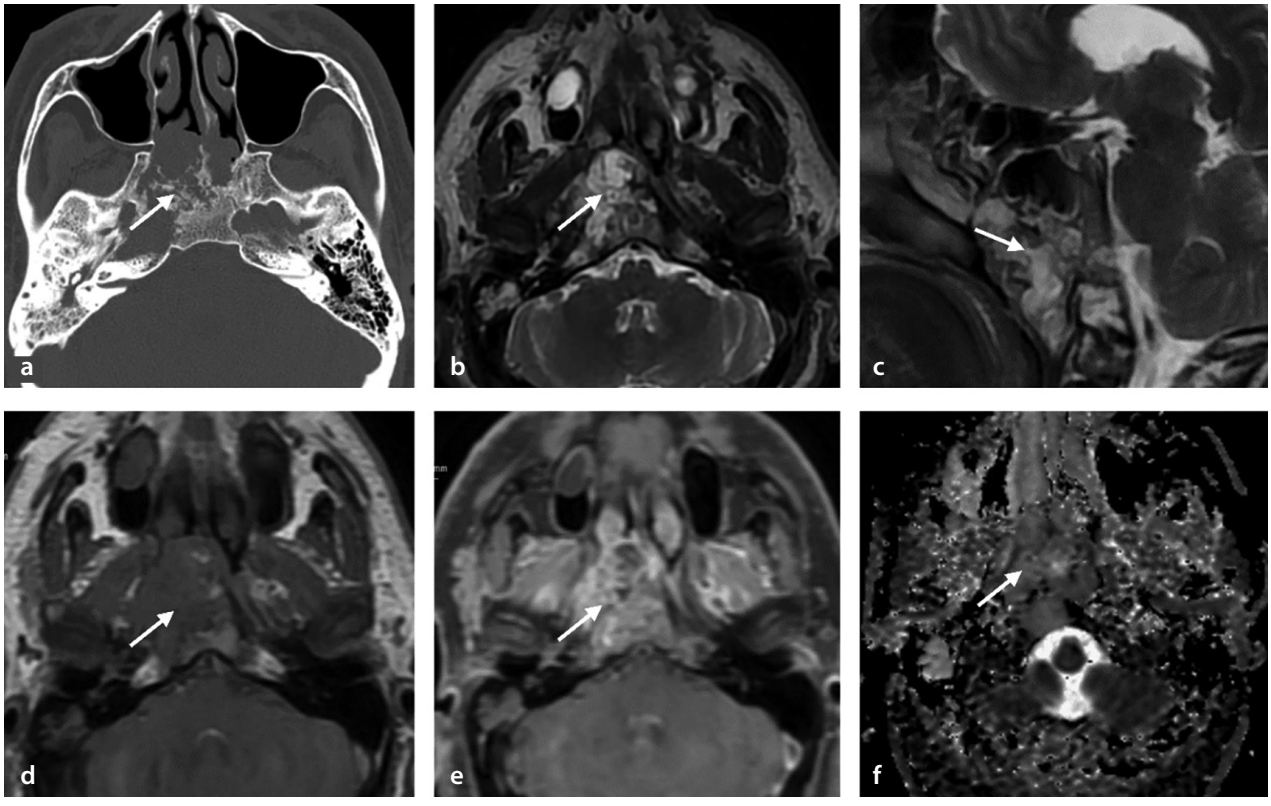

Figure 5. Imaging findings from a 60-year-old male patient who presented with hearing loss and sudden-onset diplopia, subsequently diagnosed with clival chordoma. Axial computed tomography image **(a)** reveals a lytic, destructive mass containing sequestered bone tissue (arrow). The T2-weighted magnetic resonance images **(b, c)** reveal a hyperintense lesion. The T1-weighted (T1W) image **(d)** demonstrates a hypointense lesion with hyperintense foci suggestive of hemorrhage. A post-contrast T1W image **(e)** displays moderate heterogeneous enhancement with a honeycomb-like pattern. On the apparent diffusion coefficient (ADC) map **(f)**, the ADC value is measured at 1.595×10^{-3} mm^2/sec. The patient received external beam radiotherapy following the surgical diagnosis of chordoma.

post-contrast heterogeneous enhancement with a ring-and-arc pattern (Figure 7). Chordomas should be considered in the differential diagnosis. Differentiation from chordomas is best made based on location, as chordomas arise from notochordal remnants and typically occur along the midline, whereas chondrosarcomas are typically centered on the petro-occipital fissure. Additionally, ADC values can help distinguish between the two, as chondrosarcomas generally have higher ADC values.

Treatment involves maximal safe resection followed by adjuvant radiotherapy.

Multiple myeloma

One of the diagnostic criteria for multiple myeloma is bone involvement. The most commonly affected region is the axial skeleton, particularly the vertebrae. Radiological evaluation plays a crucial role in supporting the diagnosis, excluding other causes, and identifying potential complications.

Typically, well-defined lytic bone lesions are observed in the commonly affected axial skeleton. However, one of the bone marrow involvement patterns may also present as entirely normal-appearing bone marrow.

On MRI, five active bone marrow involvement patterns have been described, including normal-appearing marrow, a focal pattern, a diffuse pattern, a salt-and-pepper (micronodular) pattern, and a combination of focal lesions within a diffuse pattern.

Active lesions are hyperintense on T2W images, hypointense on T1W images, and demonstrate enhancement on post-contrast T1W images. These lesions also demonstrate diffusion restriction (Figure 8).

The differential diagnosis includes lytic bone metastases.

Metastasis

Prostate, breast, and lung cancers account for most bone metastases. Lesions may appear as lytic, sclerotic, or mixed patterns on imaging and are often associated with bone marrow signal changes on MRI (Figure 9). Clival metastases can cause cranial nerve deficits or skull base compression symptoms, necessitating thorough radiological evaluation for an accurate diagnosis and treatment planning.

In elderly patients without a known malignancy, multiple lytic lesions raise suspicion for multiple myeloma as a key differential diagnosis. Features favoring metastases include the involvement of vertebral pedicles rather than vertebral bodies and distal ap-

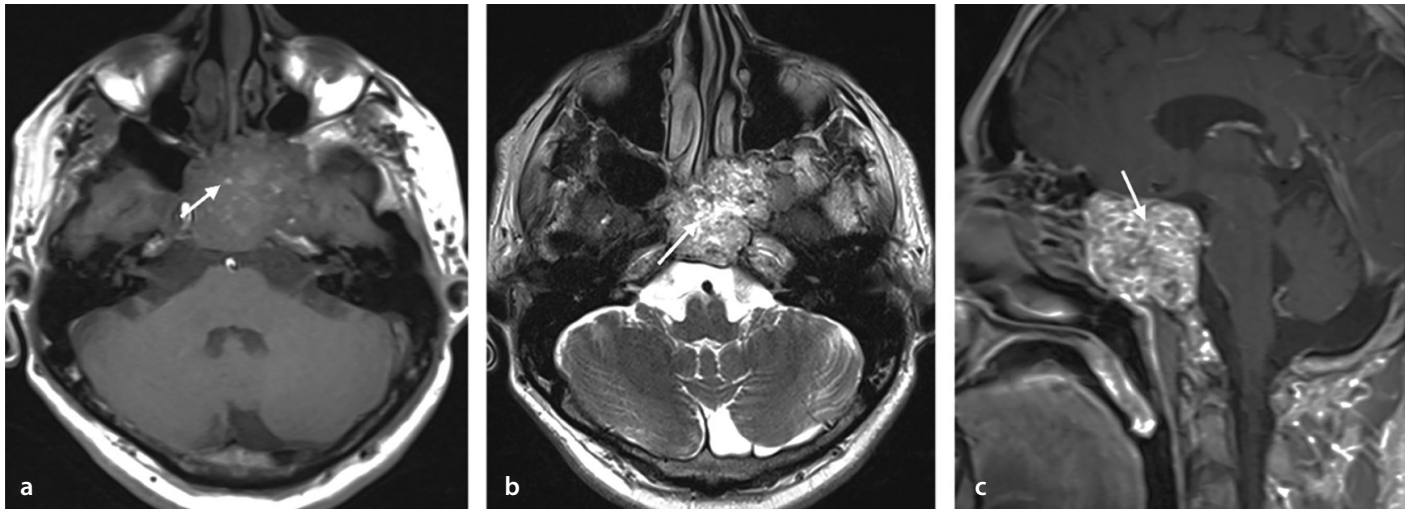

Figure 6. Magnetic resonance images of a 62-year-old male patient with a clival chordoma. The lesion appears hypointense on the T1-weighted (T1W) imaging **(a)**, with punctate hyperintense foci, hyperintense on T2-weighted imaging **(b)**, and demonstrates a honeycomb-like enhancement on post-contrast T1W imaging **(c)**, consistent with a diagnosis of clival chordoma (arrow).

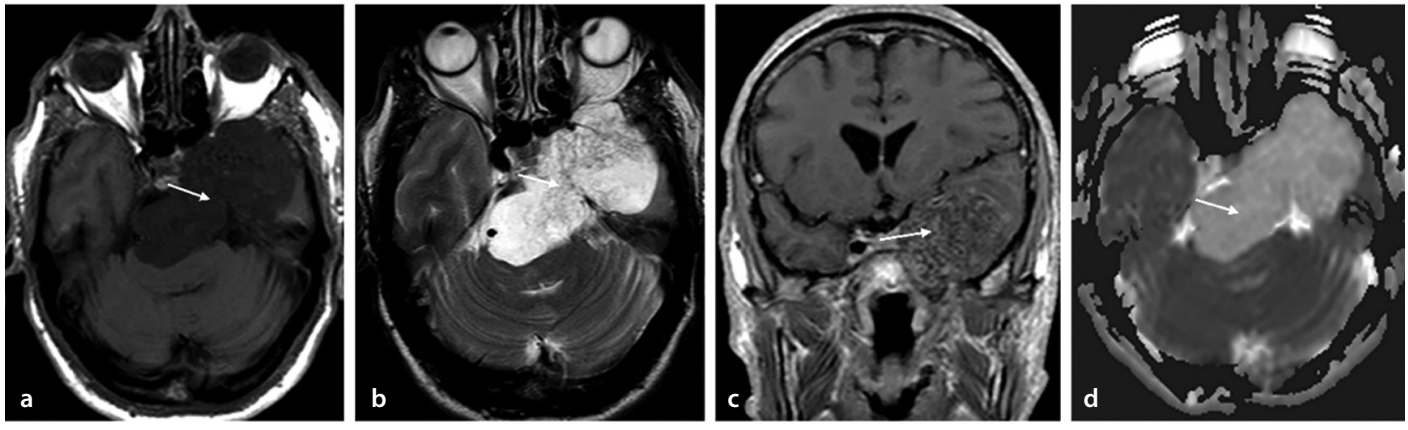

Figure 7. Magnetic resonance images of a 52-year-old male patient with chondrosarcoma. The lesion is hypointense on the T1-weighted (T1W) imaging **(a)**, hyperintense on the T2-weighted imaging **(b)**, and demonstrates septal enhancement on the post-contrast T1W imaging **(c)**. The apparent diffusion coefficient (ADC) map **(d)** reveals high ADC values (1.955×10^{-3} mm^2/sec) in this expansile mass arising from the petro-occipital synchondrosis, extending posteriorly toward the brainstem and anteriorly into the temporal region (arrow). The histopathological diagnosis confirmed chondrosarcoma.

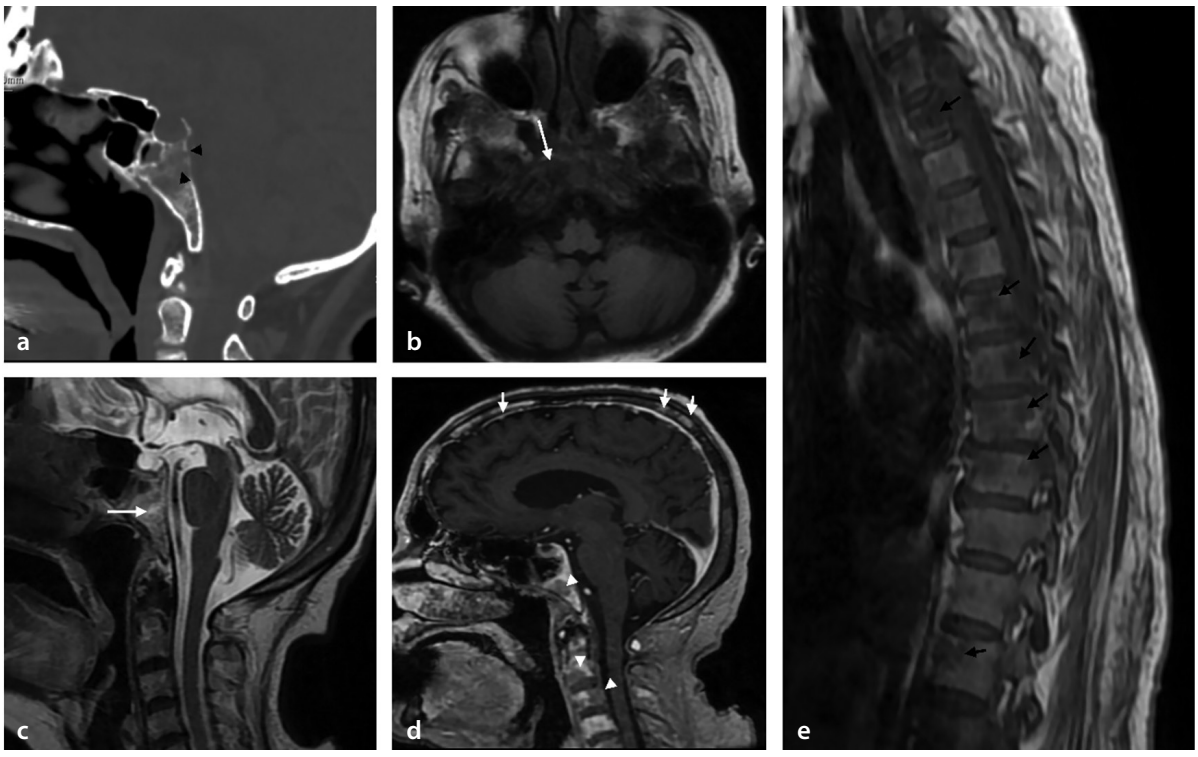

Figure 8. A 71-year-old female patient diagnosed with multiple myeloma. Computed tomography scan **(a)** reveals a lytic, destructive lesion in the clivus (black arrowhead). Axial T1-weighted (T1W) magnetic resonance imaging (MRI) **(b)** reveals the lesion as hypointense, whereas the sagittal T2-weighted MRI **(c)** demonstrates it as hyperintense (long white arrow). Post-contrast sagittal T1W MRI **(d)** reveals multiple lesions in the calvarium (short white arrows), clivus, and cervical vertebrae (white arrowheads). Sagittal T1W thoracic MRI **(e)** reveals diffuse bone marrow signal reduction with multiple focal hypointense lesions (black arrows). The combination of focal lesions within a diffuse pattern, along with bone marrow involvement, older age, and clinical-laboratory findings, supports the diagnosis of multiple myeloma.

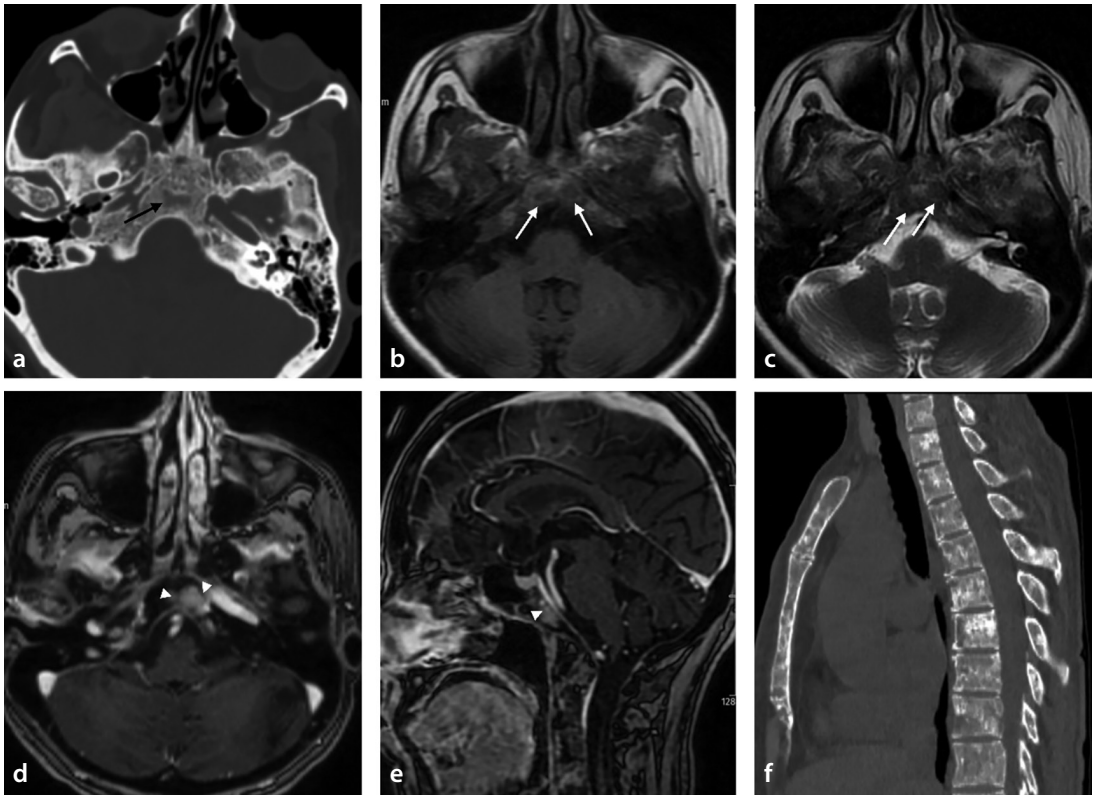

Figure 9. Images of a 60-year-old female patient diagnosed with breast cancer revealing clivus metastasis. Computed tomography (CT) scan **(a)** demonstrates a lytic lesion (black arrow). Axial T1-weighted (T1W) magnetic resonance imaging (MRI) **(b)** and T2-weighted MRI **(c)** reveal hypointense lesions (white arrows). Axial **(d)** and sagittal **(e)** post-contrast T1W images demonstrate homogeneously enhancing lesions (arrowhead). Sagittal CT image **(f)** revealing mixed lytic and sclerotic lesions consistent with mixed-type bone metastasis.

pendicular skeleton involvement. Although both conditions may exhibit variable bone scan findings on bone scintigraphy, including areas of increased (hot) or decreased (cold) uptake, extensive bone metastases rarely present with a normal scan appearance, unlike multiple myeloma.

Paraclival pathologies

Infectious and inflammatory lesions

Skull base osteomyelitis

Skull base osteomyelitis (SBO), often linked to necrotizing external otitis, is classified as lateral or central based on the infection source. Lateral SBO arises from otogenic or odontogenic infections, affecting the temporal bone and nearby structures, whereas central SBO originates from sinus infections, involving the clivus and sphenoid bones. It has an insidious onset, often presenting with delayed symptoms, such as persistent headaches and neurological deficits, after the apparent improvement of the initial otogenic infection.

CT and MRI are vital for diagnosing SBO, although imaging findings may lag behind clinical symptoms. Early bone destruction is often missed on CT, which primarily identifies skull base extension and temporomandibular joint involvement in chronic necrotizing otitis externa. MRI shows a decreased T1W signal, T2W hypointensity caused by necrosis, and diffuse post-contrast enhancement indicating extension of the infection (Figure 10). Diffusion-weighted imaging reveals higher ADC values than for malignancies (e.g., nasopharyngeal cancer, lymphoma, metastases).[13] Imaging is crucial for tracking infection spread, abscesses, and intracranial and vascular complications such as stroke, venous sinus thrombosis, or pseudoaneurysms.[14]

Differential diagnoses include nasopharyngeal carcinoma (NPC), which appears isointense to muscle on T1W images and iso- to hyperintense on T2W images, often revealing a mass with diffusion restriction, heterogeneous post-contrast enhancement, and potential perineural spread. Metastases typically exhibit variable, heterogeneous signal intensity on T1W and T2W images, with irregular post-contrast enhancement on T1W images. Lymphoma is characterized by mild hypointensity on T1W images, homogeneous hyperintensity on T2W images, and uniform post-contrast enhancement. Minor salivary gland tumors, such as in mucin-producing areas, display variable T2W signal intensity and are iso- to hypointense on T1W images with gradual post-contrast enhancement. Key MRI features, including a mass with low ADC values and cervical lymphadenopathy, assist in distinguishing malignancies; however, surgical biopsy remains essential for a definitive diagnosis.

SBO is most commonly caused by *Pseudomonas aeruginosa* in patients with diabetes and those who are immunocompromised, with *Aspergillus* as the leading fungal pathogen. Treatment involves prolonged intravenous antibiotics or antifungal therapy. Surgery is rarely performed because of the inaccessible location. Imaging may lag behind clinical recovery; therefore, treatment efficacy is primarily assessed by the resolution of the symptoms and inflammatory markers rather than imaging findings. Moreover, ^{18}F-FDG PET imaging may be used for the treatment response assessment and management guidance, especially in patients with SBO who experience treatment side effects.[15]

Secondary clival lesions: pathologies extending to the clivus

Head and neck pathologies

Nasopharyngeal carcinoma

Radiology is critical for NPC staging, treatment planning, and response monitoring, with MRI being the modality of choice because of its superior soft tissue resolution and sensitivity to perineural spread and intracranial extension. According to the American Joint Committee on Cancer tumor, node, and metastasis cancer staging system (8th edition), the involvement of bony structures (skull base, cervical vertebrae) and/or paranasal sinuses is classified as T3, with clival involvement also categorized as T3.[16]

On MRI, NPC appears isointense to muscle on T1W images and iso- to hyperintense on T2W images, with diffusion restriction, heterogeneous post-contrast enhancement, and perineural spread (Figure 11). In cases of skull base invasion, differential diagnoses include plasmacytoma, lymphoma, metastases, and other malignancies.

Sinonasal malignancies

CT is more effective for bone invasion, whereas MRI is more effective for tumor spread, dural invasion, and perineural spread, which is vital for pre-treatment staging. The T2W signal intensity varies—mucin-producing adenocarcinomas are hyperintense, whereas non-mucin tumors are iso-hypointense. On T1W images, tumors appear iso-hypointense with gradual post-contrast enhancement.

Differentiating sinonasal carcinoma from adenocarcinoma radiologically can be difficult. Sinonasal lymphoma and extramedullary plasmacytoma should be considered in the differential diagnosis. Lymphoma exhibits homogeneous enhancement, causes bone remodeling, lacks necrosis, and has a low ADC value. In our case, the differential diagnoses include sinonasal malignancy, lymphoma, and metastasis. The heterogeneous signal and enhancement, along with the lack of significant diffusion restriction, favor sinonasal malignancies over lymphoma (Figure 12).

Sinonasal carcinomas, which are locally invasive and prone to recurrence, are treated with surgery followed by adjuvant chemoradiotherapy. By contrast, lymphomas are primarily treated with chemotherapy and/or radiation therapy.

Intracranial pathologies

Pituitary neuroendocrine tumor/pituitary adenoma

Pituitary adenomas are now classified as pituitary neuroendocrine tumors (PitNETs) in the revised fifth edition of the World Health Organization classification. Their behavior code has changed from "0" (benign) to "3" (malignant). Most PitNETs are benign, with a recurrence rate of less than 5% after surgery, requiring minimal further treatment. Aggressive PitNETs are rare, accounting for less than 1% of cases.[17]

Clival invasion by PitNETs occurs in 8.2% of cases, usually by direct extension, whereas extrasellar PitNETs, originating from the clivus, account for 7.2%.[18,19] PitNETs should be considered in the differential diagnosis of clival masses.

The MRI signal intensity of PitNETs varies depending on degeneration, hemorrhage, or infarction. Moreover, T1W images exhibit mild hypointensity or isointensity, whereas T2W images exhibit variable signal intensities. On contrast-enhanced MRI, PitNETs are typically hypointense or isointense compared with the pituitary gland (Figure 13). Imaging strategies depend on tumor size and hormonal activity.

Meningiomas

Bone involvement may result from hyperostosis, neoplastic infiltration, or prima-

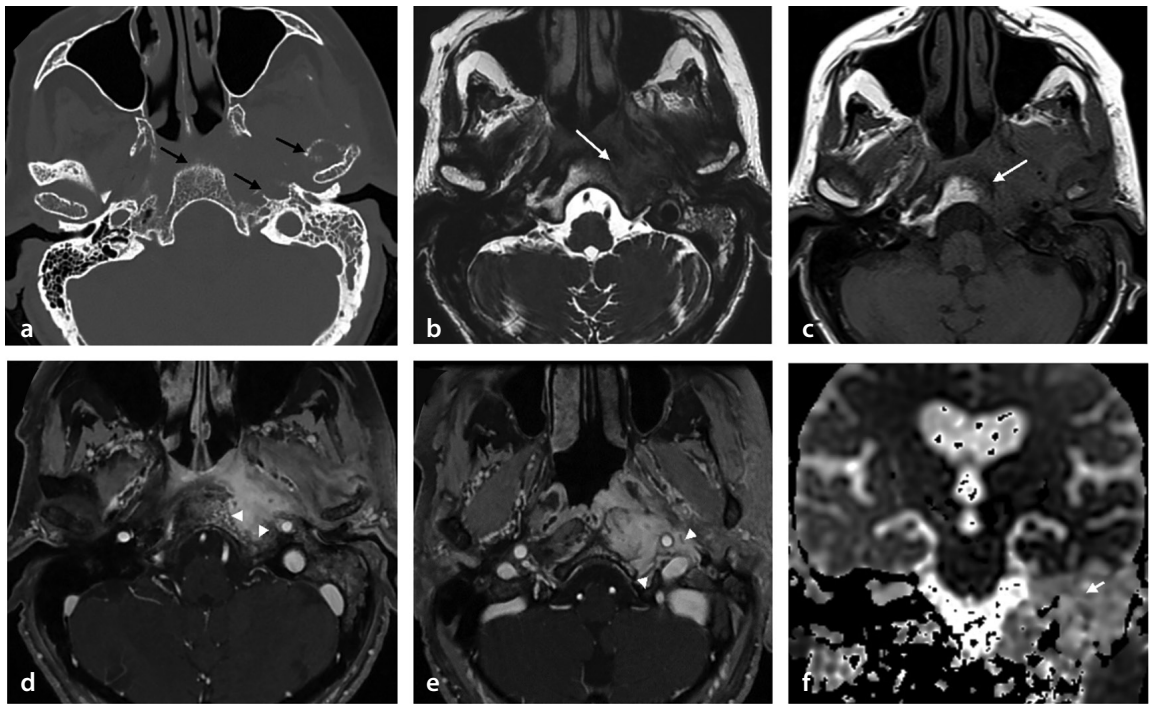

Figure 10. Imaging findings consistent with necrotizing otitis externa and skull base osteomyelitis in a 67-year-old female patient with a history of diabetes mellitus, presenting with prolonged severe ear pain. Computed tomography **(a)** reveals opacification in the mastoid and middle ear, along with erosion of the clivus, mandibular condyle, and temporal bone (black arrows). Axial heavily T2-weighted image **(b)** demonstrates slight hyperintensity, and non-fat-saturated T1-weighted (T1W) images **(c)** reveal reduced bone marrow signal (white arrow). Post-contrast fat-saturated T1W images **(d, e)** reveal clival invasion with extension into the pharyngeal mucosal area, parapharyngeal, and carotid space (arrowheads). The apparent diffusion coefficient (ADC) map **(f)** demonstrates hyperintensity and high ADC values (small arrow). The patient's ear culture grew *Pseudomonas aeruginosa*, and intravenous treatment is ongoing.

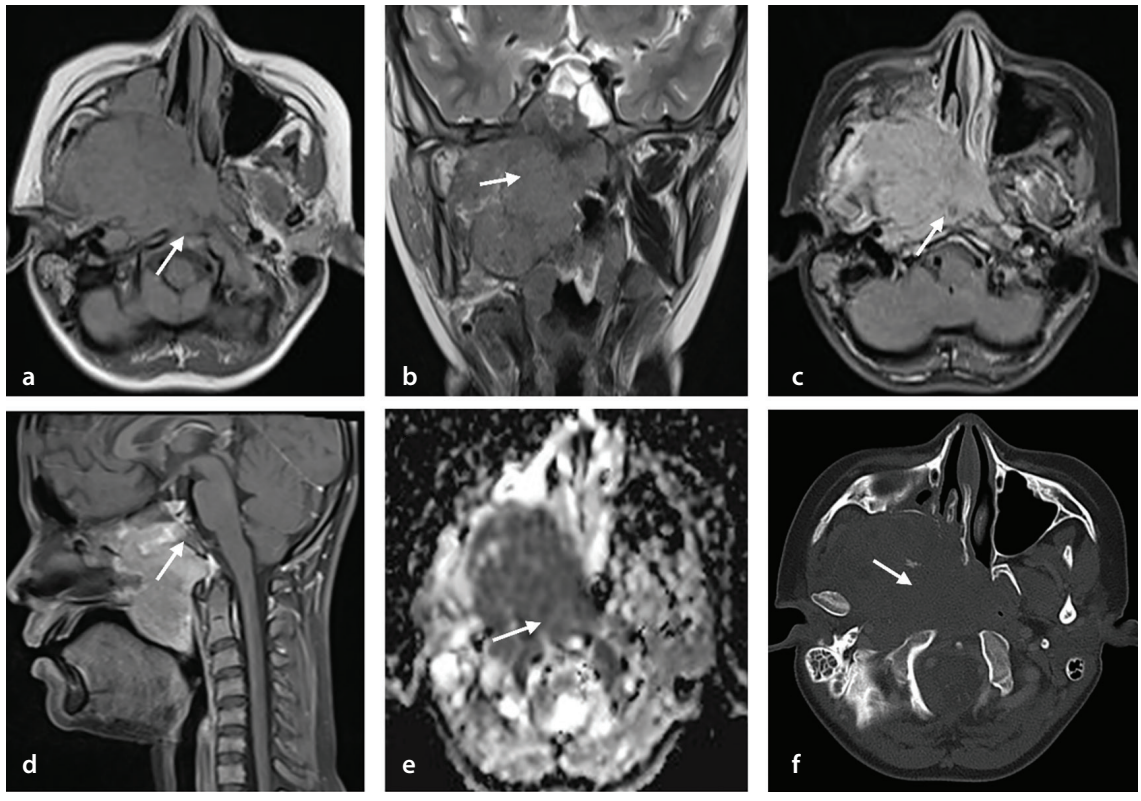

Figure 11. Imaging findings in a 14-year-old male patient diagnosed with T4 stage nasopharyngeal carcinoma. Magnetic resonance imaging reveals a mass that is isointense on T1-weighted images **(a)**, iso-hyperintense on T2-weighted images **(b)**, and has heterogeneous, marked contrast enhancement on post-contrast axial **(c)** and sagittal **(d)** images. It has low apparent diffusion coefficient values **(e)**. The histopathological diagnosis was nasopharyngeal carcinoma, classified as T4 stage nasopharyngeal carcinoma according to the American Joint Committee on Cancer tumor, node, metastasis classification system (8th edition). Computed tomography imaging **(f)** reveals extensive erosion of bony structures and skull base invasion.

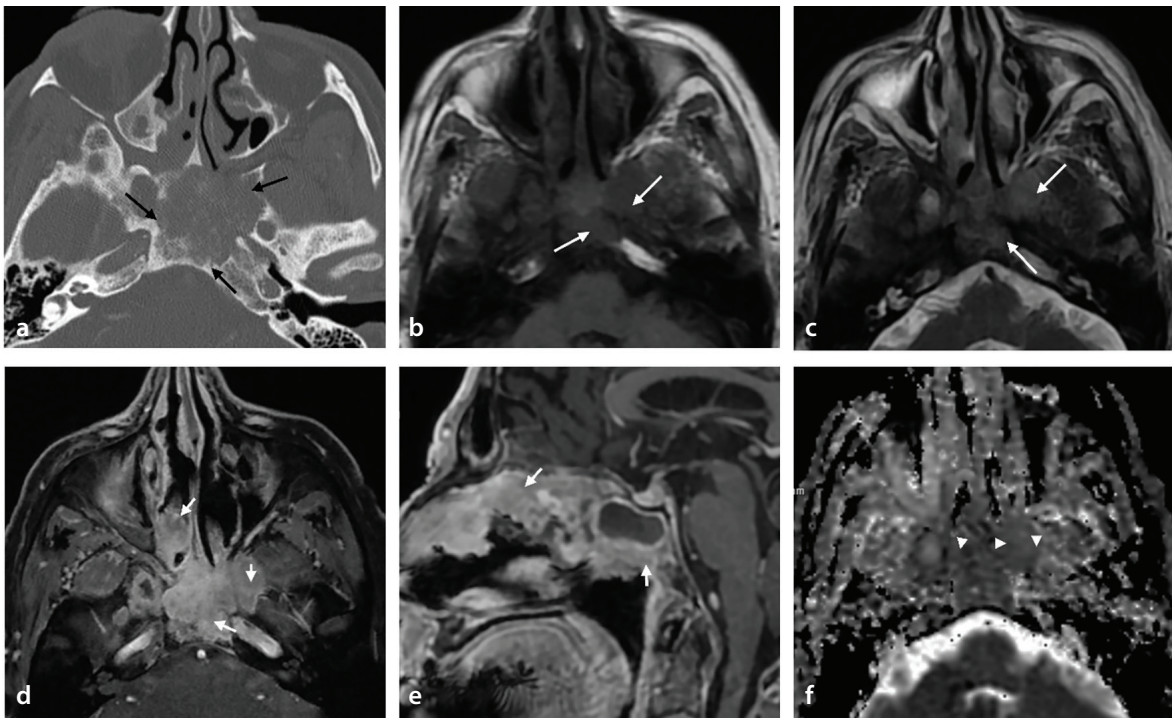

Figure 12. Imaging findings in a 72-year-old male patient presenting with strabismus and diplopia diagnosed with sinonasal mucoepidermoid carcinoma. Computed tomography images **(a)** reveal sclerosis and a lytic destructive appearance extending to the clivus in the sphenoid bone (black arrows). Magnetic resonance imaging reveals the lesion as iso-hypointense on T1-weighted (T1W) **(b)** and slightly hyperintense signal on T2-weighted **(c)** sequences (white arrows). Post-contrast T1W axial **(d)** and sagittal **(e)** images demonstrate invasion from the sphenoid sinus to the sphenoid wing, nasal cavity, cavernous sinuses, and skull base (short arrows). The apparent diffusion coefficient (ADC) map **(f)** reveals hypointensity and low ADC values (arrowheads). Histopathological examination confirmed high-grade mucoepidermoid carcinoma. The patient is undergoing concurrent chemoradiotherapy after surgery.

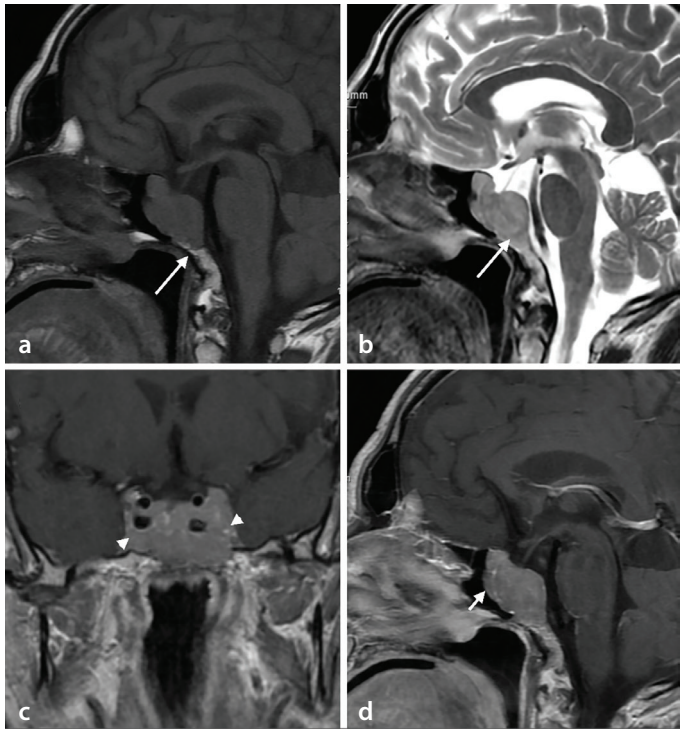

Figure 13. Magnetic resonance images (MRI) of a 43-year-old male patient presenting with headache and dizziness, revealing a pituitary neuroendocrine tumor (macroadenoma) invading the clivus. On MRIs, the lesion appears hypointense on T1-weighted (T1W) **(a)** and hyperintense on T2-weighted **(b)** images, invading the clivus (long arrow). The post-contrast T1W coronal image **(c)** demonstrates invasion of the cavernous sinuses (arrowhead), and the sagittal image **(d)** reveals indentation into the sphenoid sinus (short arrow) with mild contrast enhancement of the sellar mass. The lesion was histopathologically diagnosed as a pituitary neuroendocrine tumor.

ry intraosseous meningioma, which is rare, comprising 2%–2.4% of all meningiomas.[20] It typically affects the frontal and parietal bones, with clival involvement being uncommon.

Most intraosseous meningiomas are osteoblastic, causing hyperostosis and occasionally mimicking fibrous dysplasia. In rare cases, they present as osteolytic lesions. CT typically reveals hyperostosis, with occasional lytic lesions. On MRI, the lesion is hypointense on T1W images, isointense with the cortex on T2W images, and demonstrates homogeneous enhancement on post-contrast images (Figures 14 and 15).

Differential diagnoses include Paget's disease, fibrous dysplasia, osteoma for osteoblastic forms, and metastasis and plasmacytoma for osteolytic forms. Skull base meningiomas should also be differentiated from perineural spread in head and neck malignancies.

Meningiomas grow slowly, with surgery as the primary treatment, using approaches such as endoscopic endonasal, middle fossa, or posterior fossa surgery. Radiation therapy is added for partial or subtotal resection.

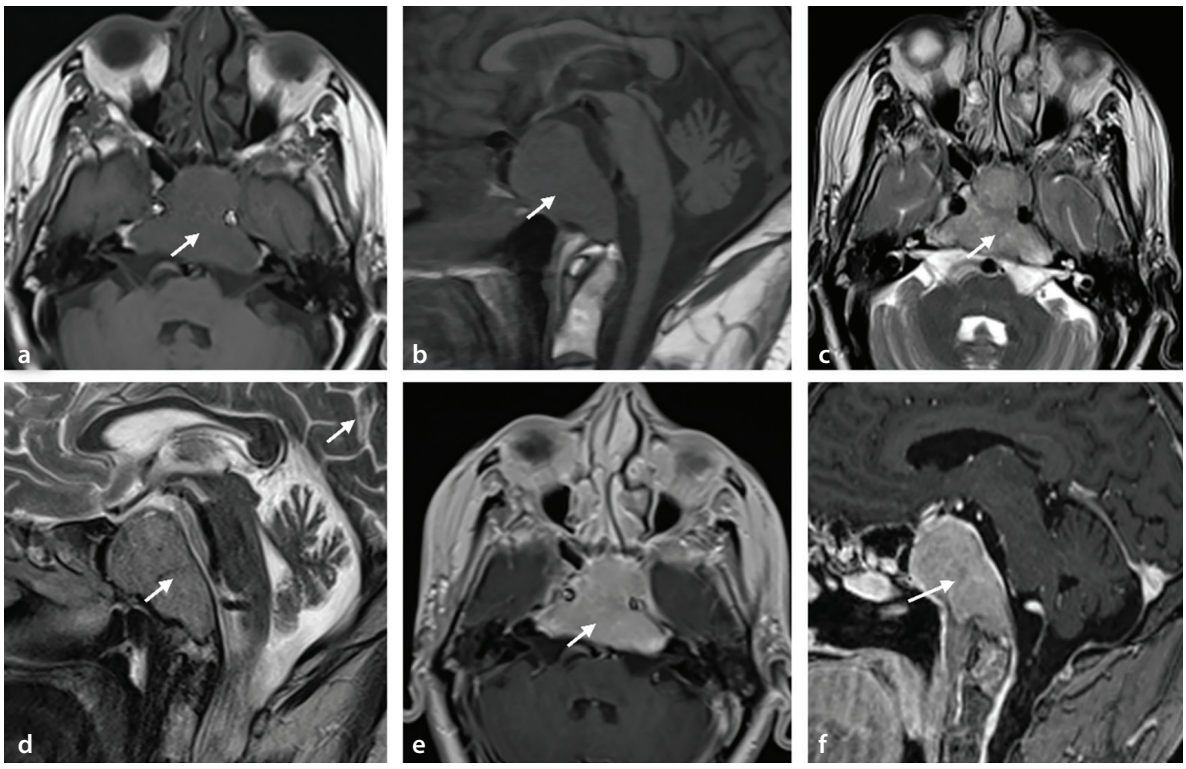

Figure 14. Magnetic resonance images of a 57-year-old male patient presenting with headache and restricted gaze, diagnosed with clival meningioma. The lesion (arrows) appears iso-hypointense on axial **(a)** and sagittal **(b)** T1-weighted (T1W) images and isointense on axial **(c)** and sagittal **(d)** T2-weighted images. Post-contrast T1W axial **(e)** and sagittal **(f)** images demonstrate homogeneous contrast enhancement of the clival mass, which extends laterally to the left cavernous sinus, anteriorly to the sphenoid sinus, and posteriorly to the prepontine cistern. Following the diagnosis of meningioma, the patient underwent radiotherapy.

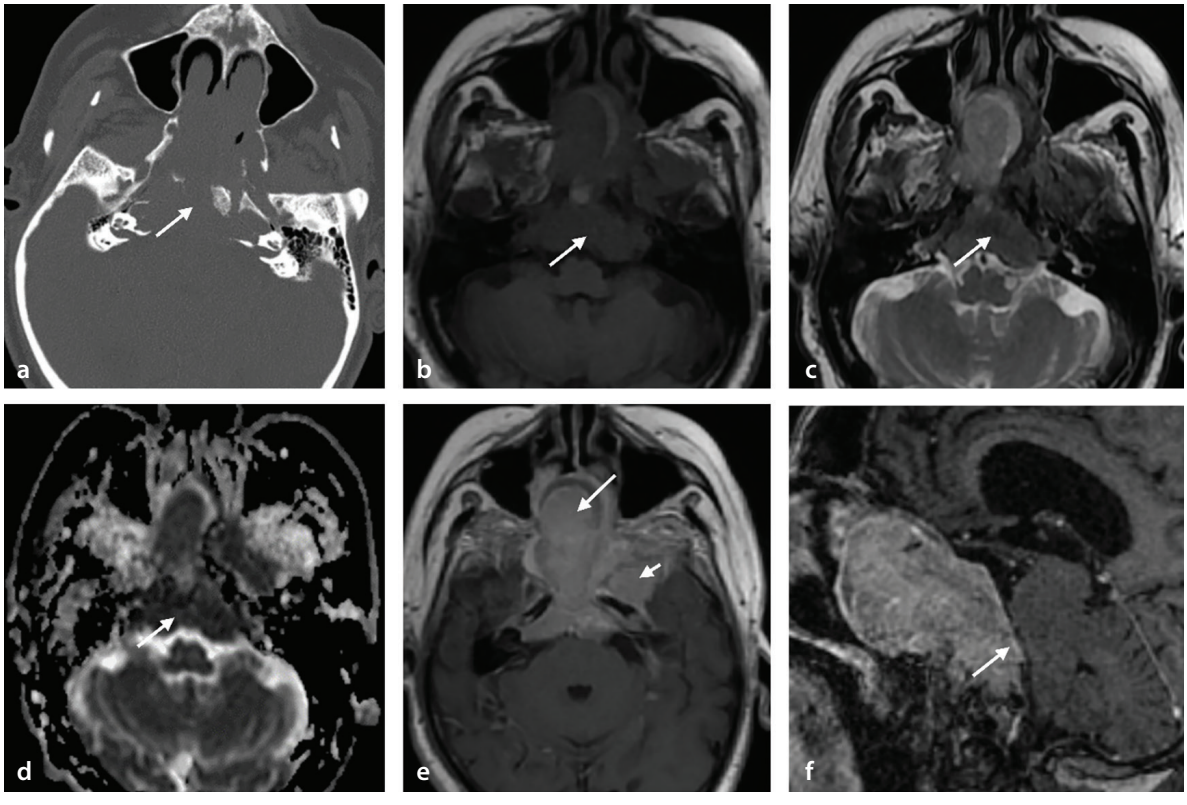

Figure 15. Radiological images of a 74-year-old male patient presenting with nausea, vomiting, and left eyelid ptosis, diagnosed with atypical meningioma (World Health Organization grade 2) invading the clivus. The computed tomography scan **(a)** reveals a lytic expansile lesion, whereas the lesion appears isointense on T1-weighted **(b)** and T2-weighted **(c)** images, with low apparent diffusion coefficient (ADC) values on the ADC map **(d)**. Post-contrast images **(e, f)** demonstrate homogeneous contrast enhancement of the expansile clival lesion (arrow). The lesion invades the right sphenoid sinus, extends bilaterally into the parasellar region, reaches the masticator space on the left, and posteriorly extends into the prepontine cistern.

Conclusion

This pictorial essay underscores the critical role of imaging in diagnosing and differentiating clival and paraclival pathologies. Comprehensive radiologic evaluation using advanced MRI and CT techniques facilitates accurate characterization, aiding in optimal management strategies. Understanding the imaging features and their clinical correlations is essential for diagnosing these complex conditions.

Conflict of interest disclosure

The authors declared no conflicts of interest.

References

1. McDonald SW, Miller J. When does the spheno-occipital synchondrosis close? *Clin Anat*. 2022;35(4):512-525. [CrossRef]
2. Kimura F, Kim KW, Friedman H, Russell EJ, Breit R. MR imaging of the normal and abnormal clivus. *Am J Roentgenol*. 1990;155(6):1285-1291. [CrossRef]
3. Adrien M, Nadège B, William K. Mazabraud's syndrome. *J Belgian Soc Radiol*. 2022;106(1):71. [CrossRef]
4. Kinnunen AR, Sironen R, Sipola P. Magnetic resonance imaging characteristics in patients with histopathologically proven fibrous dysplasia—a systematic review. *Skeletal Radiol*. 2020;49(6):837-845. [CrossRef]
5. Nkie VE, Martin S. Fibrous dysplasia of the clivus: case report and literature review. *Cureus*. 2023;15(9):45417. [CrossRef]
6. Choi JH, Ro JY. The 2020 WHO classification of tumors of bone: an updated review. *Adv Anat Pathol*. 2021;28(3):119-138. [CrossRef]
7. Stevens AR, Branstetter BF, Gardner P, Pearce TM, Zenonos GA, Arani K. Ecchordosis physaliphora: does it even exist? *AJNR Am J Neuroradiol*. 2023;44(8):889-893. [CrossRef]
8. Özgür A, Esen K, Kara E, et al. Ecchordosis physaliphora: evaluation with precontrast and contrast-enhanced fast imaging employing steady-state acquisition MR imaging based on proposed new classification. *Clin Neuroradiol*. 2016;26(3):347-353. [CrossRef]
9. Lee SH, Kwok KY, Wong SM, Chan CXJ, Wong YT, Tsang ML. Chordoma at the skull base, spine, and sacrum: a pictorial essay. *J Clin Imaging Sci*. 2022;12:44. [CrossRef]
10. Das P, Soni P, Jones J, et al. Descriptive epidemiology of chordomas in the United States. *J Neurooncol*. 2020;148(1):173-178. [CrossRef]
11. Welzel T, Meyerhof E, Uhl M, et al. Diagnostic accuracy of DW MR imaging in the differentiation of chordomas and chondrosarcomas of the skull base: a 3.0-T MRI study of 105 cases. *Eur J Radiol*. 2018;105:119-124. [CrossRef]
12. Kremenevski N, Schlaffer SM, Coras R, Kinfe TM, Graillon T, Buchfelder M. Skull base chordomas and chondrosarcomas. *Neuroendocrinology*. 2020;110(9-10):836-847. [CrossRef]
13. Ozgen B, Oguz KK, Cila A. Diffusion MR imaging features of skull base osteomyelitis compared with skull base malignancy. *Am J Neuroradiol*. 2011;32(1):179-184. [CrossRef]
14. Jain N, Jasper A, Vanjare HA, Mannam P, Mani SE. The role of imaging in skull base osteomyelitis - reviewed. *Clin Imaging*. 2020;67:62-67. [CrossRef]
15. Saxena A, Subramanyam P, Sarma M, Bhad B, Bhaskaran R, Palaniswamy SS. 18F-FDG PET imaging for treatment response assessment and management guidance in patients with skull base osteomyelitis. *Nucl Med Commun*. 2024;45(7):589-600. [CrossRef]
16. Amin MB, Greene FL, Edge SB, et al. The eighth edition AJCC cancer staging manual: continuing to build a bridge from a population-based to a more "personalized" approach to cancer staging. *CA Cancer J Clin*. 2017;67(2):93-99. [CrossRef]
17. Tsukamoto T, Miki Y. Imaging of pituitary tumors: an update with the 5th WHO Classifications-part 1. Pituitary neuroendocrine tumor (PitNET)/pituitary adenoma. *Jpn J Radiol*. 2023;41(8):789-806. [CrossRef]
18. Tajudeen BA, Kuan EC, Adappa ND, et al. Ectopic pituitary adenomas presenting as sphenoid or clival lesions: case series and management recommendations. *J Neurol Surg B Skull Base*. 2017;78(2):120-124. [CrossRef]
19. Chen X, Dai J, Ai L, et al. Clival invasion on multidetector CT in 390 pituitary macroadenomas: Correlation with sex, subtype and rates of operative complication and recurrence. *AJNR Am J Neuroradiol*. 2011;32(4):785-789. [CrossRef]
20. Butscheidt S, Ernst M, Rolvien T, et al. Primary intraosseous meningioma: clinical, histological, and differential diagnostic aspects. *J Neurosurg*. 2020;133(2):281-290. [CrossRef]